43. Underwater Robotics

Gianluca Antonelli, Thor I. Fossen, Dana R. Yoerger

This chapter deals with the main underwater robotic topics. First, a brief introduction showing the constantly expanding role of marine robotics in oceanic engineering is given; this section also contains some historical backgrounds. Most of the following sections strongly overlap with the corresponding chapters presented in this handbook; hence, to avoid useless repetitions, only those aspects peculiar to the underwater environment are discussed, assuming that the reader is already familiar with concepts such as fault detection systems when discussing the corresponding underwater implementation. The modeling section is presented by focusing on a coefficient-based approach capturing the most relevant underwater dynamic effects. Two sections dealing with the description of the sensor and the actuating systems are then given. Autonomous underwater vehicles require the implementation of mission control system as well as guidance and control algorithms. Underwater localization is also discussed. Underwater manipulation is then briefly approached. Fault detection and fault tolerance, together with the coordination control of multiple underwater vehicles, conclude the theoretical part of the chapter. Two final sections, reporting some successful applications and discussing future perspectives, conclude the chapter.

43.1 The Expanding Role of Marine Robotics in Oceanic Engineering

The world's oceans cover 2/3 of the Earth's surface and have been critical to human welfare throughout history. As in ancient times, they enable the transport of goods between nations. Presently, the seas represent critical sources of food and other resources such as oil and gas. In the near term, we may soon see the emergence of offshore mining for metals as well as the exploitation of gas hydrates. Conversely, the ocean can also threaten human safety and damage infrastructure through natural phenomena such as hurricanes and tsunamis.

Our scientific understanding of the deep sea is expanding rapidly through the use of a variety of technologies. The first scientific explorations were conducted primarily through the use of diving and human-occupied submersibles, complemented by a variety of other technologies such as towed or lowered instruments, trawls, dredges, autonomous seafloor instruments, and deep-sea drilling. More recently remotely operated and autonomous vehicles have begun to revolutionize seafloor exploration, often returning superior data at reduced costs. In the near future, seafloor observatories linked by fiber-optic cables and satellites will return massive amounts of data from coastal and deep-sea sites. These observations will complement those

Fig. 43.1 The ROV Jason 2 (courtesy of the Woods Hole Oceanographic Institute, http://www.whoi.edu)

from conventional expeditionary investigations, and will require teleoperated or robotic intervention during installation and for service. An example of a remotely operated vehicle developed for the scientific study of the seafloor is the Jason 2 vehicle developed at the Woods Hole Oceanographic Institution (shown in Fig. 43.1), and a list of remotely operated vehicles for scientific exploration appears in Table 43.1 (the last vehicle in the table, Kaiko, was lost several years ago).

Table 43.1 ROVs for scientific use

Vehicle	Depth (m)	Institution	Manufacturer
Hyperdolphin	3000	JAMSTEC[a]	ISE
Dolphin 3K	3000	JAMSTEC	JAMSTEC
Quest	4000	MARUM[b]	Shilling
Tiburon	4000	MBARI[c]	MBARI
ROPOS	5000	CSSF[d]	ISE
Victor	6000	IFREMER[e]	IFREMER
Jason	6500	WHOI[f]	WHOI
ISIS	6500	NOC[g]	WHOI
UROV 7K	7000	JAMSTEC	JAMSTEC
Kaiko	11000	JAMSTEC	JAMSTEC

[a] Japan Marine. Science and Technology Center
[b] Zentrum für Marine Umweltwissenschaften
[c] Monterey Bay Aquarium Research Institute
[d] Canadian Scientific Submersile Facility
[e] Institut français de recherche pourl'exploitation de la mer
[f] Woods Hole Oceanographic Institution
[g] National Oceanography Centre

Offshore oil and gas installations are presently serviced almost exclusively by remotely operated vehicles (ROVs), physically connected via a tether to receive power and data, with human divers used only for the shallowest installations. Subsea systems require extensive work capability during installation, and need frequent inspection and intervention to support drilling operations, actuate valves, repair or replace subsea components, and to accomplish a variety of tasks required to maintain production rates and product quality. The trend toward robotic and teleoperated subsea intervention is certain to continue as offshore oil and gas production moves into deeper waters, and economic considerations push key production steps from surface platforms to the seafloor. Remotely operated manipulators enable these systems to perform complex tasks such as debris removal, cleaning using abrasive tools, and to operate a variety of nondestructive testing tools. The effectiveness of using ROVs decreases with depth mainly due to the cost increase and the difficulties of handling the long tether.

Autonomous underwater vehicles (AUVs) are free-swimming unoccupied underwater vehicles that can overcome the limitations imposed by ROV tethers for some tasks. Such vehicles carry their own energy supplies (presently batteries, perhaps fuel cells in the future) and communicate only through acoustics and perhaps optical links in the near future. Limited communications require these vehicles to operate independently of continuous human control, in many cases the vehicles operate completely autonomously. AUVs are currently used for scientific survey tasks, oceanographic sampling, underwater archeology and under-ice survey. Military applications, such as mine detection and landing site survey, are presently operational, and more ambitious applications such as long-term undersea surveillance are in engineering development. Presently, AUVs are incapable of sampling or manipulations tasks like those done routinely by ROVs, as typical work environments tend to be complex and challenging even to skilled human pilots.

Today, approximately 200 AUVs are operational, many of them experimental. However, they are maturing rapidly. Recently several companies now offer commercial services with AUVs. As an example, for the oil and gas industry the cost reduction of a survey performed with an AUVs instead of a towed vehicle is up to 30% and the data quality is generally higher. Likewise, commercial manufacturers in several countries now offer turnkey AUV systems for specific, well-defined tasks. Currently, remotely operated manipulators are standard

equipment for most ROVs, while on the contrary autonomous manipulation is still a research challenge; the two projects SAUVIM [43.1] and ALIVE [43.2] were devoted to studying this control problem.

43.1.1 Historical Background

Boats have been used by humans since the start of recorded history, but vehicles able to go under water are more recent. Perhaps the first recorded idea of an underwater machine came from Aristotle; according to legend he built the: *skaphe andros* (boat-man) that allowed Alexander the Great (Alexander III of Macedonia, 356–323 BC) to stay submerged for at least half a day during the war of Tiro in 325 BC. This is probably unrealistic; if true it would precede Archimedes' law, which was first articulated in approximately 250 BC. Leonardo Da Vinci may have been the first to design an underwater vehicle. His efforts were recorded in the *Codice Atlantico* (*Codex Atlanticus*), written between 1480 and 1518. Legends say that Leonardo worked on the idea of an underwater military machine but he destroyed the results as he judged them to be too dangerous. The first use of feedback theory for marine control was probably the Northseeking device, patented in 1908, that used gyroscopic principals to develop the first autopilot [43.3]. From that point on, the use of feedback theory in marine control grew continuously; it is interesting to notice that the proportional–integral–derivative (PID) control commonly used today in numerous industrial applications was first formally analyzed in 1929 by Minorsky [43.4]. The first remotely operated underwater vehicle, POODLE, was built in 1953, and the ROV evolved through the 1960s and 1970s, mostly for military purposes. In the 1980s ROVs became established for use in the commercial offshore industry and began to emerge for scientific applications. The first tetherless, autonomous vehicles were built for experimental purposes in the 1970s. Currently, AUVs are becoming increasingly commonplace for scientific, military, and commercial applications. Turnkey AUV systems for a range of tasks are available from commercial vendors, and AUV services can be acquired from a number of companies [43.5].

43.2 Underwater Robotics

43.2.1 Modeling

A rigid body is completely described by its position and orientation with respect to a reference frame Σ_i, $O_i - xyz$ that is supposed to be Earth-fixed and inertial. Let us define $\boldsymbol{\eta}_1 \in \mathbb{R}^3$ as

$$\boldsymbol{\eta}_1 = (x \;\; y \;\; z)^\top ,$$

the vector of the body position coordinates in an Earth-fixed reference frame. The vector $\dot{\boldsymbol{\eta}}_1$ is the corresponding time derivative (expressed in the Earth-fixed frame). If one defines

$$\boldsymbol{\nu}_1 = (u \;\; v \;\; w)^\top$$

as the linear velocity of the origin of the body-fixed frame Σ_b, $O_\mathrm{b} - x_\mathrm{b}\, y_\mathrm{b}\, z_\mathrm{b}$ with respect to the origin of the Earth-fixed frame expressed in the body-fixed frame (from now on: body-fixed linear velocity) the following relation between the defined linear velocities holds

$$\boldsymbol{\nu}_1 = \boldsymbol{R}_\mathrm{I}^\mathrm{B} \dot{\boldsymbol{\eta}}_1 , \tag{43.1}$$

where $\boldsymbol{R}_\mathrm{I}^\mathrm{B}$ is the rotation matrix expressing the transformation from the inertial frame to the body-fixed frame.

Let us define $\boldsymbol{\eta}_2 \in \mathbb{R}^3$ as

$$\boldsymbol{\eta}_2 = (\phi \;\; \theta \;\; \psi)^\top$$

the vector of body Euler angle coordinates in a Earth-fixed reference frame. In the nautical field those are commonly named roll, pitch, and yaw. Yaw is defined as rotation around the z axis of the fixed frame; pitch is defined as rotation around the y axis resulting after the yaw movement; and roll is defined as rotation around the x axis resulting after both yaw and pitch movements. The vector $\dot{\boldsymbol{\eta}}_2$ is the corresponding time derivative (expressed in the inertial frame). Let us define

$$\boldsymbol{\nu}_2 = (p \;\; q \;\; r)^\top$$

as the angular velocity of the body-fixed frame with respect to the Earth-fixed frame expressed in the body-fixed frame (from now on: body-fixed angular velocity). The vector $\dot{\boldsymbol{\eta}}_2$ does not have a physical interpretation and it is related to the body-fixed angular velocity by a proper Jacobian matrix

$$\boldsymbol{\nu}_2 = \boldsymbol{J}_{k,o}(\boldsymbol{\eta}_2)\dot{\boldsymbol{\eta}}_2 . \tag{43.2}$$

Table 43.2 Common notation for the motion of a marine vehicle

		Forces and moments	$\boldsymbol{\nu}_1, \boldsymbol{\nu}_2$	$\boldsymbol{\eta}_1, \boldsymbol{\eta}_2$
Motion in the x-direction	Surge	X	u	x
Motion in the y-direction	Sway	Y	v	y
Motion in the z-direction	Heave	Z	w	z
Rotation about the x-axis	Roll	K	p	ϕ
Rotation about the y-axis	Pitch	M	q	θ
Rotation about the z-axis	Yaw	N	r	ψ

The matrix $\boldsymbol{J}_{k,o} \in \mathbb{R}^{3\times3}$ can be expressed in terms of the Euler angles as

$$\boldsymbol{J}_{k,o}(\boldsymbol{\eta}_2) = \begin{pmatrix} 1 & 0 & -s_\theta \\ 0 & c_\phi & c_\theta s_\phi \\ 0 & -s_\phi & c_\theta c_\phi \end{pmatrix} , \tag{43.3}$$

where c_α and s_α are abbreviations for $\cos(\alpha)$ and $\sin(\alpha)$, respectively. The matrix $\boldsymbol{J}_{k,o}(\boldsymbol{\eta}_2)$ is not invertible for every value of $\boldsymbol{\eta}_2$. In detail, it is

$$\boldsymbol{J}_{k,o}^{-1}(\boldsymbol{\eta}_2) = \frac{1}{c_\theta} \begin{pmatrix} 1 & s_\phi s_\theta & c_\phi s_\theta \\ 0 & c_\phi c_\theta & -c_\theta s_\phi \\ 0 & s_\phi & c_\phi \end{pmatrix} , \tag{43.4}$$

that it is singular for $\theta = (2l+1)\pi/2\,\text{rad}$, with $l \in \mathbb{N}$, i. e., for a pitch angle of $\pm\pi/2\,\text{rad}$.

The rotation matrix $\boldsymbol{R}_\text{I}^\text{B}$, needed in (43.1) to transform the linear velocities, is expressed in terms of the Euler angles by

$$\boldsymbol{R}_\text{I}^\text{B}(\boldsymbol{\eta}_2) = \begin{pmatrix} c_\psi c_\theta & s_\psi c_\theta & -s_\theta \\ -s_\psi c_\phi + c_\psi s_\theta s_\phi & c_\psi c_\phi + s_\psi s_\theta s_\phi & s_\phi c_\theta \\ s_\psi s_\phi + c_\psi s_\theta c_\phi & -c_\psi s_\phi + s_\psi s_\theta c_\phi & c_\phi c_\theta \end{pmatrix} . \tag{43.5}$$

Table 43.2 shows the common notation used for marine vehicles according to the Society of Naval Architects and Marine Engineers (SNAME) notation [43.6]; a sketch is shown in Fig. 43.2.

As for any representation of a rigid body's orientation several possibilities arise, among them, the use

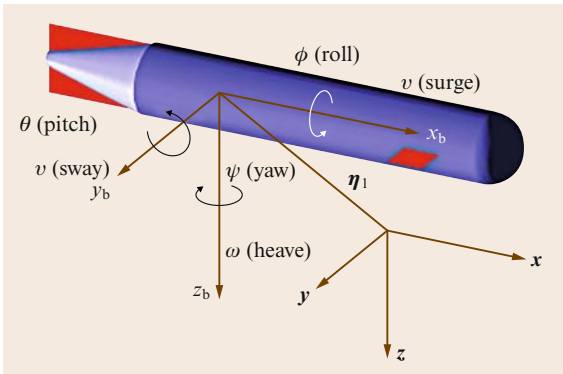

Fig. 43.2 Motion variables for an underwater vehicle

of a four-parameter description given by quaternions. The term *quaternion* was introduced by Hamilton in 1840, 70 years after the introduction of a four-parameter rigid-body attitude representation by Euler. An introduction to alternative orientation representations can be found in Chap. 1 and concerning the marine environment in [43.7].

It is useful to collect the kinematic equations in six-dimensional matrix forms. Let us define the vector $\boldsymbol{\eta} \in \mathbb{R}^6$ as

$$\boldsymbol{\eta} = \begin{pmatrix} \boldsymbol{\eta}_1 \\ \boldsymbol{\eta}_2 \end{pmatrix} \tag{43.6}$$

and the vector $\boldsymbol{\nu} \in \mathbb{R}^6$ as

$$\boldsymbol{\nu} = \begin{pmatrix} \boldsymbol{\nu}_1 \\ \boldsymbol{\nu}_2 \end{pmatrix} , \tag{43.7}$$

and, defining the matrix $\boldsymbol{J}_\text{e}(\boldsymbol{R}_\text{B}^\text{I}) \in \mathbb{R}^{6\times6}$

$$\boldsymbol{J}_\text{e}(\boldsymbol{R}_\text{B}^\text{I}) = \begin{pmatrix} \boldsymbol{R}_\text{I}^\text{B} & \boldsymbol{0}_{3\times3} \\ \boldsymbol{0}_{3\times3} & \boldsymbol{J}_{k,o} \end{pmatrix} , \tag{43.8}$$

where the rotation matrix $\boldsymbol{R}_\text{I}^\text{B}$ is given in (43.5) and $\boldsymbol{J}_{k,o}$ is given in (43.3),

$$\boldsymbol{\nu} = \boldsymbol{J}_\text{e}(\boldsymbol{R}_\text{B}^\text{I})\dot{\boldsymbol{\eta}} . \tag{43.9}$$

The inverse mapping, given the block-diagonal structure of $\boldsymbol{J}_\text{e}$, is given by

$$\dot{\boldsymbol{\eta}} = \boldsymbol{J}_\text{e}^{-1}(\boldsymbol{R}_\text{B}^\text{I})\boldsymbol{\nu} = \begin{pmatrix} \boldsymbol{R}_\text{B}^\text{I} & \boldsymbol{0}_{3\times3} \\ \boldsymbol{0}_{3\times3} & \boldsymbol{J}_{k,o}^{-1} \end{pmatrix} \boldsymbol{\nu} , \tag{43.10}$$

where $\boldsymbol{J}_{k,o}^{-1}$ is given in (43.4).

Defining as

$$\boldsymbol{\tau}_{\mathrm{v}} = \begin{pmatrix} \boldsymbol{\tau}_1 \\ \boldsymbol{\tau}_2 \end{pmatrix} ,$$

the vector of generalized forces, where

$$\boldsymbol{\tau}_1 = (X \;\; Y \;\; Z)^{\top} , \tag{43.11}$$

the resultant forces acting on the rigid body expressed in a body-fixed frame, and

$$\boldsymbol{\tau}_2 = (K \;\; M \;\; N)^{\top} , \tag{43.12}$$

the corresponding resultant moment to the pole O_{b}, it is possible to rewrite the Newton–Euler equations of motion of a rigid body moving in the space as:

$$\boldsymbol{M}_{\mathrm{RB}}\dot{\boldsymbol{\nu}} + \boldsymbol{C}_{\mathrm{RB}}(\boldsymbol{\nu})\boldsymbol{\nu} = \boldsymbol{\tau}_{\mathrm{v}} . \tag{43.13}$$

The derivation of (43.13) can be found in Chap. 2.

The matrix $\boldsymbol{M}_{\mathrm{RB}}$ is constant, symmetric, and positive definite, i. e., $\dot{\boldsymbol{M}}_{\mathrm{RB}} = \boldsymbol{0}$ and $\boldsymbol{M}_{\mathrm{RB}} = \boldsymbol{M}_{\mathrm{RB}}^{\top} > \boldsymbol{0}$. Its unique parametrization is of the form

$$\boldsymbol{M}_{\mathrm{RB}} = \begin{pmatrix} m\boldsymbol{I}_3 & -m\boldsymbol{S}(\boldsymbol{r}_C^{\mathrm{b}}) \\ m\boldsymbol{S}(\boldsymbol{r}_{\mathrm{C}}^{\mathrm{b}}) & \boldsymbol{I}_{O_{\mathrm{b}}} \end{pmatrix} , \tag{43.14}$$

where $\boldsymbol{r}_{\mathrm{C}}^{\mathrm{b}}$ is the 3×1 distance vector to the center of gravity (CG) expressed in the body-fixed frame, $\boldsymbol{I}_3$ is the 3×3 identity matrix, and $\boldsymbol{I}_{O_{\mathrm{b}}}$ is the inertia tensor expressed in the body-fixed frame $\boldsymbol{S}(\boldsymbol{x})$ is the matrix operator performing the cross product between two (3×1) vectors

$$\boldsymbol{S}(\boldsymbol{x}) = \begin{pmatrix} 0 & -x_3 & x_2 \\ x_3 & 0 & -x_1 \\ -x_2 & x_1 & 0 \end{pmatrix} .$$

On the other hand, there does not exist a unique parametrization of the matrix $\boldsymbol{C}_{\mathrm{RB}}$, which represents the Coriolis and centripetal terms. It can be demonstrated that the matrix $\boldsymbol{C}_{\mathrm{RB}}$ can always be parameterized such that it is skew symmetric, i. e.,

$$\boldsymbol{C}_{\mathrm{RB}}(\boldsymbol{\nu}) = -\boldsymbol{C}_{\mathrm{RB}}^{\top}(\boldsymbol{\nu}) \qquad \forall \boldsymbol{\nu} \in \mathbb{R}^6 ; \tag{43.15}$$

explicit expressions for $\boldsymbol{C}_{\mathrm{RB}}$ can be found in [43.7].

Notice that (43.13) can be greatly simplified if the origin of the body-fixed frame is chosen to be coincident with the central frame, i. e., $\boldsymbol{r}_{\mathrm{C}}^{\mathrm{b}} = \boldsymbol{0}$.

Hydrodynamic Generalized Forces

Equation (43.13) represents the motion of a rigid body in an empty space, while dealing with ships or underwater vehicles requires the consideration of the presence of the hydrodynamics generalized forces, i. e., the forces and moments caused by the presence of the fluid. In hydrodynamics it is common to assume that the generalized hydrodynamics forces on a rigid body can be linearly superimposed [43.8]; in particular, those are separated into radiation-induced forces, environmental disturbances, and restoring forces due to gravity and buoyancy.

Radiation-induced forces are defined as the *forces on the body when the body is forced to oscillate with the wave excitation frequency and there are no incident waves*; these can be identified as the sum of the *added mass* due to the inertia of the surrounding fluid and the *radiation-induced potential damping* due to the energy dissipated by generated surface waves.

Environmental disturbances can be identified as the generalized forces caused by the wind, the waves, and the ocean current.

The overall equations of motions can therefore be written in matrix form as [43.7, 9, 10]:

$$\boldsymbol{M}_{\mathrm{v}}\dot{\boldsymbol{\nu}} + \boldsymbol{C}_{\mathrm{v}}(\boldsymbol{\nu})\boldsymbol{\nu} + \boldsymbol{D}_{\mathrm{v}}(\boldsymbol{\nu})\boldsymbol{\nu} + \boldsymbol{g}_{\mathrm{v}}(\boldsymbol{R}_{\mathrm{B}}^{\mathrm{I}}) = \boldsymbol{\tau}_{\mathrm{v}} , \tag{43.16}$$

where $\boldsymbol{M}_{\mathrm{v}} = \boldsymbol{M}_{\mathrm{RB}} + \boldsymbol{M}_{\mathrm{A}}$ and $\boldsymbol{C}_{\mathrm{v}} = \boldsymbol{C}_{\mathrm{RB}} + \boldsymbol{C}_{\mathrm{A}}$ also include the added mass terms.

In the following subsections these generalized forces, specific to the marine environment, will be briefly discussed.

Added Mass and Inertia

When a rigid body is moving in a fluid, the additional inertia of the fluid surrounding the body that is accelerated by the movement of the body has to be considered. This effect can be neglected in industrial robotics since the density of the air is much lower than the density of a moving mechanical system. In underwater applications, however, the density of the water, $\rho \approx 1000\,\mathrm{kg/m^3}$, is comparable with the density of the vehicles. In particular, at 0 °C, the density of freshwater is $1002.68\,\mathrm{kg/m^3}$; for sea water with 3.5% salinity it is $\rho = 1028.48\,\mathrm{kg/m^3}$.

The fluid surrounding the body is accelerated with the body, so a force is necessary to achieve this acceleration, while the fluid exerts a reaction force which is equal in magnitude and opposite in direction. This reaction force is the added mass contribution. The added mass is not a quantity of fluid to add to the system such that it has an increased mass. Different properties hold with respect to the 6×6 inertia matrix of a rigid body due to the fact that the added mass is a function of the body's surface geometry.

The hydrodynamic force along $\boldsymbol{x}_\mathrm{b}$ due to the linear acceleration in the $\boldsymbol{x}_\mathrm{b}$-direction is defined as:

$$X_\mathrm{A} := -X_{\dot{u}}\dot{u}\,, \qquad \text{where} \qquad X_{\dot{u}} := \frac{\partial X}{\partial \dot{u}}\,,$$

where the symbol ∂ denotes the partial derivative. In the same way it is possible to define all the remaining 35 elements that relate the six force/moment components $(X\ Y\ Z\ K\ M\ N)^\top$ to the six linear/angular accelerations $(\dot{u}\ \dot{v}\ \dot{w}\ \dot{p}\ \dot{q}\ \dot{r})^\top$. These elements can be grouped into the added mass matrix $\boldsymbol{M}_\mathrm{A} \in \mathbb{R}^{6\times 6}$. Usually, all the elements of the matrix are nonzero.

In general, added mass and potential damping will be frequency dependent and depend on the forward speed. This is also the case for certain viscous damping terms (skin friction, roll damping, etc.). This gives a pseudo differential equation describing the frequency response of the vehicle. Since some of the coefficients depend on the frequency this is not an ordinary differential equation (ODE). The frequency equation, however, can be transformed to the time domain using the concepts described in [43.11] and [43.12], and recently in [43.13]. The resulting equation is an ODE where the added inertia matrix $\boldsymbol{M}_\mathrm{A}$ is constant, speed independent, and positive definite:

$$\boldsymbol{M}_\mathrm{A} = \boldsymbol{M}_\mathrm{A}^\top > \boldsymbol{0}\,, \quad \dot{\boldsymbol{M}}_\mathrm{A} = \boldsymbol{0}\,. \tag{43.17}$$

This result is well known from ship hydrodynamics; see [43.14] for instance. The matrix $\boldsymbol{M}_\mathrm{A}$ can be computed using numerical programs such as WAMIT or Matlab, based on the US Air Force Digital Datcom [43.15]; in this case, the infinity-frequency result should be used, that is, $\boldsymbol{M}_\mathrm{A} = \boldsymbol{A}(\infty)$ where $\boldsymbol{A}(\omega)$ is the frequency-dependent added mass matrix. The potential damping matrix will be small compared to the viscous effects and drag/lift terms. Hence, this term can be set to zero for underwater vehicles. If the added mass is computed experimentally, it is common practice to symmetrize the results such that

$$\boldsymbol{M}_\mathrm{A} = \frac{1}{2}\left(\boldsymbol{A}_\mathrm{exp} + \boldsymbol{A}_\mathrm{exp}^\top\right)\,,$$

where $\boldsymbol{A}_\mathrm{exp}$ denotes the experimentally obtained added mass terms.

If the body is completely submerged in the water and is designed with port/starboard symmetry (xz-plane) as is common for underwater vehicles in six degrees-of-freedom (DOFs), the following structure of the matrices $\boldsymbol{M}_\mathrm{A}$ can be considered:

$$\boldsymbol{M}_\mathrm{A} = -\begin{pmatrix} X_{\dot{u}} & 0 & X_{\dot{w}} & 0 & X_{\dot{q}} & 0 \\ 0 & Y_{\dot{v}} & 0 & Y_{\dot{p}} & 0 & Y_{\dot{r}} \\ Z_{\dot{u}} & 0 & Z_{\dot{w}} & 0 & Z_{\dot{q}} & 0 \\ 0 & K_{\dot{v}} & 0 & K_{\dot{p}} & 0 & K_{\dot{r}} \\ M_{\dot{u}} & 0 & M_{\dot{w}} & 0 & M_{\dot{q}} & 0 \\ 0 & N_{\dot{v}} & 0 & N_{\dot{p}} & 0 & N_{\dot{r}} \end{pmatrix}. \tag{43.18}$$

The added mass coefficients can theoretically be derived by exploiting the geometry of the rigid body or numerically by strip theory [43.16].

In [43.17] the coefficients for the experimental AUV Phoenix of the Naval Postgraduate School (NPS) are reported. These coefficients have been derived experimentally, and the geometry gives a nondiagonal $\boldsymbol{M}_\mathrm{A}$ matrix. To provide an order of magnitude for the added mass terms, for the vehicle mass of about 5000 kg, the $X_{\dot{u}}$ is approximately -500 kg.

The added mass also makes an *added* Coriolis and centripetal contribution. It can be demonstrated that the matrix expression can always be parameterized such that

$$\boldsymbol{C}_\mathrm{A}(\boldsymbol{\nu}) = -\boldsymbol{C}_\mathrm{A}^\top(\boldsymbol{\nu})\,, \qquad \forall \boldsymbol{\nu} \in \mathbb{R}^6\,,$$

whose symbolic expressions can be found in [43.3].

Hydrodynamic Damping

The hydrodynamic damping for marine vehicles is mainly caused by

- potential damping
- skin friction
- wave drift damping
- vortex shedding damping
- viscous damping

The radiation-induced potential damping due to forced body oscillations is commonly known as potential damping; its dynamic contribution is usually negligible with respect to, e.g., the viscous friction for underwater vehicles while it may be significant for surface vessels.

Linear skin friction is due to laminar boundary layers and can affect the low-frequency motion of the vehicle. Together with this effect, at high frequencies it is possible to observe a quadratic, or nonlinear, skin friction phenomenon caused by turbulent boundary layers.

Wave drift damping is the dominant dynamic damping effect in surge motion of surface vessels in high sea. It can be considered as an added resistance for boats advancing in waves; its drift is proportional to the square of the significant wave height. In the sway and yaw di-

Table 43.3 Lift and drag coefficient for a cylinder

Reynolds number	Regime motion	C_d	C_l
$R_n < 2\times10^5$	Subcritical flow	1	3–0.6
$2\times10^5 < R_n < 5\times10^5$	Critical flow	1–0.4	0.6
$5\times10^5 < R_n < 3\times10^5$	Transcritical flow	0.4	0.6

rections, however, its dynamic contribution is negligible with respect to the effect of vortex shedding.

A body moving in a fluid causes a separation of the flow; this can still be considered as laminar in the upstream while two antisymmetric vortices can be observed in the downstream. In case that the body is a cylinder moving in a direction normal to its axis, the result is a periodic force normal to both the velocity and the axis. This effect may cause the oscillation of cables and other underwater structures. However, concerning underwater vehicles, this effect is negligible for ROVs and may be counteracted by designing proper small control surfaces for torpedo-like AUVs.

Vortex shedding is an unsteady flow that takes place at special flow velocities (according to the size and shape of the cylindrical body). In this flow vortices are created at the back of the body, periodically from each side.

The viscosity of the fluid also causes dissipative forces. These are composed of drag and lift forces, the former being parallel to the relative velocity of the vehicle with respect to the water while the latter are normal to it. For a sphere moving in a fluid, the drag force can be modeled as [43.8]

$$F_{\text{drag}} = \frac{1}{2}\rho U^2 S C_d(R_n)\,, \tag{43.19}$$

where ρ is the fluid density, U is the velocity of the sphere, S is the frontal area of the sphere, C_d is the nondimensional drag coefficient, and R_n is the Reynolds number. For a generic body, S is the projection of the frontal area along the flow direction. The drag force can be considered as the sum of two physical effects: the frictional contribution of the surface whose normal is perpendicular to the flow velocity, and the pressure contribution of the surface whose normal is parallel to the flow velocity. For a hydrofoil moving in a fluid, the lift force can be modeled as [43.8]

$$F_{\text{lift}} = \frac{1}{2}\rho U^2 S C_l(R_n, \alpha)\,, \tag{43.20}$$

where S is now the area, C_l is the nondimensional lift coefficient, and α is the angle of attack, i. e., the angle between the relative velocity and the tangent to the surface. For small angles of attack, i. e., $|\alpha| < 10°$, the lift coefficient is approximatively proportional to α and rapidly decays to zero as α increases [43.18].

The drag and lift coefficients are therefore dependent on the Reynolds number, i. e., on the laminar/turbulent fluid motion

$$R_n = \frac{\rho|U|D}{\mu}\,,$$

where D is the characteristic dimension of the body perpendicular to the direction of U and μ is the dynamic viscosity of the fluid. Table 43.3 reports the drag coefficients as a function of the Reynolds number for a cylinder [43.19].

A common simplification considers only linear and quadratic damping terms and group these into a matrix $\boldsymbol{D}_v$ as in (43.16) such that

$$\boldsymbol{D}_v(\boldsymbol{\nu}) > \boldsymbol{0}\,, \qquad \forall \boldsymbol{\nu} \in \mathbb{R}^6\,.$$

Gravity and Buoyancy

When a rigid body is completely or partially submerged in a fluid under the effect of the gravity two more forces have to be considered: the gravitational force and buoyancy. The latter is the only hydrostatic effect, i. e., it is not a function of the relative movement between the body and fluid.

Let us define as

$$\boldsymbol{g}^I = (0\ \ 0\ \ 9.81)^\top \text{m/s}^2$$

the acceleration of gravity. This effect is not constant but varies with depth, longitude, and latitude; however, this value is usually accurate enough for most applications except for inertial navigation systems.

For a completely submerged body the computation of these dynamic effects is straightforward. The submerged weight of the body is defined as $W = m\|\boldsymbol{g}^I\|$, while its buoyancy $B = \rho\nabla\|\boldsymbol{g}^I\|$, where ∇ is the volume of the body and m is its mass. The gravity force, which acts at the center of mass $\boldsymbol{r}_C^B$, is represented in the body-fixed frame by

$$\boldsymbol{f}_G(\boldsymbol{R}_I^B) = \boldsymbol{R}_I^B \begin{pmatrix} 0 \\ 0 \\ W \end{pmatrix}\,,$$

while the buoyancy force, acting at the center of buoyancy $\boldsymbol{r}_B^B$, is represented in the body-fixed frame by

$$\boldsymbol{f}_B(\boldsymbol{R}_I^B) = -\boldsymbol{R}_I^B \begin{pmatrix} 0 \\ 0 \\ B \end{pmatrix}\,.$$

The 6×1 vector of force/moment due to gravity and buoyancy in the body-fixed frame, included in the left-hand side of the equations of motion, is represented by

$$\boldsymbol{g}_{\mathrm{v}}(\boldsymbol{R}_{\mathrm{I}}^{\mathrm{B}}) = -\begin{pmatrix} \boldsymbol{f}_{\mathrm{G}}(\boldsymbol{R}_{\mathrm{I}}^{\mathrm{B}}) + \boldsymbol{f}_{\mathrm{B}}(\boldsymbol{R}_{\mathrm{I}}^{\mathrm{B}}) \\ \boldsymbol{r}_{\mathrm{G}}^{\mathrm{B}} \times \boldsymbol{f}_{\mathrm{G}}(\boldsymbol{R}_{\mathrm{I}}^{\mathrm{B}}) + \boldsymbol{r}_{\mathrm{B}}^{\mathrm{B}} \times \boldsymbol{f}_{\mathrm{B}}(\boldsymbol{R}_{\mathrm{I}}^{\mathrm{B}}) \end{pmatrix} .$$

In the following, the symbol $\boldsymbol{r}_{\mathrm{G}}^{\mathrm{B}} = (x_{\mathrm{G}} \;\; y_{\mathrm{G}} \;\; z_{\mathrm{G}})^{\top}$ (with $\boldsymbol{r}_{\mathrm{G}}^{\mathrm{B}} = \boldsymbol{r}_{\mathrm{C}}^{\mathrm{B}}$) will be used for the center of gravity. The expression for $\boldsymbol{g}_{\mathrm{v}}$ in terms of the Euler angles is

$$\boldsymbol{g}_{\mathrm{v}}(\boldsymbol{\eta}_2) = \begin{pmatrix} (W-B)s_\theta \\ -(W-B)c_\theta s_\phi \\ -(W-B)c_\theta c_\phi \\ -(y_{\mathrm{G}}W - y_{\mathrm{B}}B)c_\theta c_\phi + (z_{\mathrm{G}}W - z_{\mathrm{B}}B)c_\theta s_\phi \\ (z_{\mathrm{G}}W - z_{\mathrm{B}}B)s_\theta + (x_{\mathrm{G}}W - x_{\mathrm{B}}B)c_\theta c_\phi \\ -(x_{\mathrm{G}}W - x_{\mathrm{B}}B)c_\theta s_\phi - (y_{\mathrm{G}}W - y_{\mathrm{B}}B)s_\theta \end{pmatrix} . \tag{43.21}$$

Current

Ocean currents are mainly caused by tidal movement, the atmospheric wind system over the sea surface, heat exchange at the sea surface, salinity changes, the Coriolis force due to the Earth's rotation, nonlinear waves, the major ocean circulations such as the Gulf Stream, the effect of setup phenomena or storm surges, and strong density gradients in the upper ocean. Currents can be very different due to local climatic and/or geographic characteristics; as an example, in fjords, the tidal effect can cause currents of up to 3 m/s, moreover, specific mathematical models exist for the various components [43.7].

Let us assume that the ocean current, expressed in the inertial frame, $\boldsymbol{v}_{\mathrm{c}}^{\mathrm{I}}$, is constant and irrotational, i. e.,

$$\boldsymbol{v}_{\mathrm{c}}^{\mathrm{I}} = (v_{\mathrm{c},x} \;\; v_{\mathrm{c},y} \;\; v_{\mathrm{c},z} \;\; 0 \;\; 0 \;\; 0)^{\top}$$

and $\dot{\boldsymbol{v}}_{\mathrm{c}}^{\mathrm{I}} = \boldsymbol{0}$; its effects can be added to the dynamics of a rigid body moving in a fluid simply by considering the *relative* velocity in the body-fixed frame

$$\boldsymbol{v}_{\mathrm{r}} = \boldsymbol{v} - \boldsymbol{R}_{\mathrm{I}}^{\mathrm{B}} \boldsymbol{v}_{\mathrm{c}}^{\mathrm{I}} \tag{43.22}$$

in the derivation of the added Coriolis and centripetal and the damping terms.

$$\boldsymbol{M}_{\mathrm{v}}\dot{\boldsymbol{v}} + \boldsymbol{C}_{\mathrm{RB}}(\boldsymbol{v})\boldsymbol{v} + \boldsymbol{C}_{\mathrm{A}}(\boldsymbol{v}_{\mathrm{r}})\boldsymbol{v}_{\mathrm{r}} + \boldsymbol{D}_{\mathrm{v}}(\boldsymbol{v}_{\mathrm{r}})\boldsymbol{v}_{\mathrm{r}} + \boldsymbol{g}_{\mathrm{v}}(\boldsymbol{R}_{\mathrm{B}}^{\mathrm{I}}) = \boldsymbol{\tau}_{\mathrm{v}} . \tag{43.23}$$

Notice that the term $\boldsymbol{C}_{\mathrm{A}}(\boldsymbol{v}_{\mathrm{r}})\boldsymbol{v}_{\mathrm{r}}$ includes the important destabilizing effect known as the Munk moment [43.8].

If $\boldsymbol{D}_{\mathrm{v}}(\boldsymbol{v}_{\mathrm{r}})$ is unknown, quadratic surge resistance and the cross-flow drag principle can be used to describe the dissipative forces and moments in surge, sway, and yaw [43.8]. Moreover:

$$\boldsymbol{C}_{\mathrm{A}}(\boldsymbol{v}_{\mathrm{r}})\boldsymbol{v}_{\mathrm{r}} + \boldsymbol{D}_{\mathrm{v}}(\boldsymbol{v}_{\mathrm{r}})\boldsymbol{v}_{\mathrm{r}} \approx (X_{\mathrm{c}} \;\; Y_{\mathrm{c}} \;\; 0 \;\; 0 \;\; 0 \;\; N_{\mathrm{c}})^{\top} ; \tag{43.24}$$

for large relative current angles $|\beta_{\mathrm{c}} - \psi|$, where β_{c} is the current direction, the cross-flow principles models the sway force Y_{c} and yaw moment N_{c} as

$$Y_{\mathrm{c}} = \frac{\rho}{2} \int_L H(x) C_{\mathrm{D}}(x) v_{\mathrm{r}}^x(x) \left| v_{\mathrm{r}}^x(x) \right| \mathrm{d}x \tag{43.25}$$

$$N_{\mathrm{c}} = \frac{\rho}{2} \int_L x H(x) C_{\mathrm{D}}(x) v_{\mathrm{r}}^x(x) \left| v_{\mathrm{r}}^x(x) \right| \mathrm{d}x , \tag{43.26}$$

where L is the vehicle length, $H(x)$ is the vehicle height, $C_{\mathrm{D}}(x)$ is the two-dimensional drag coefficient, and $v_{\mathrm{r}}^x(x) = v_{\mathrm{r}} + rx$ is the relative cross-flow velocity at x. In practice $C_{\mathrm{D}}(x)$ can be chosen as a constant between 0 and 1. The proper value can be determined by curve fitting of experimental data. Along the surge direction, however, the quadratic damping contribution X_{c} is still well represented by a term proportional to the square of the relative velocity, whose symbolic expression can be written as

$$X_{\mathrm{c}} = -X_{u|u|} u_{\mathrm{r}} |u_{\mathrm{r}}| , \tag{43.27}$$

where $-X_{u|u|} > 0$ is the quadratic surge damping coefficient, which can be found by curve fitting of experimental data or relating it to the drag coefficient C_{d} as in (43.19).

Alternatively, the computation of the quadratic surge resistance, nonlinear roll damping, and the cross-flow drag effect can be made by resorting to the Datcom database for aircraft, as shown in [43.20].

Model Properties

For completely submerged bodies in an ideal fluid moving at low velocity where there are no currents or waves, (43.16) satisfies the following properties:

- the inertia matrix is symmetric and positive definite, i. e.,
$$\boldsymbol{M}_{\mathrm{v}} = \boldsymbol{M}_{\mathrm{v}}^{\top} > \boldsymbol{0} ;$$
- the damping matrix is positive definite, i. e.,
$$\boldsymbol{D}_{\mathrm{v}}(\boldsymbol{v}) > \boldsymbol{0} ;$$

- the matrix $\boldsymbol{C}_{\mathrm{v}}(\boldsymbol{\nu})$ is skew symmetric, i. e.,

$$\boldsymbol{C}_{\mathrm{v}}(\boldsymbol{\nu}) = -\boldsymbol{C}_{\mathrm{v}}^{\top}(\boldsymbol{\nu}), \forall \boldsymbol{\nu} \in \mathbb{R}^6 .$$

Hydrodynamic Modeling

The mathematical model of an underwater robot as expressed in (43.16) is of great importance; even when simplified it captures the most important part of the dynamics. Moreover, it is in a form appropriate for control design. A wide literature exists on AUV/ROV controllers whose stability relies on the properties reported above. On the other hand, there are working conditions in which these assumptions are no longer valid, i. e., when the AUV is traveling at high speed, or close to the surface, or when its shape does not allow geometric simplifications. The latter is the case of, e.g., several ROVs. In addition, it is still common to design the controllers for AUVs based on linearized models and to control ROVs with simple PID controllers.

These considerations justify a modeling effort to calculate the hydrodynamic terms more accurately with the aim of prediction, simulation, and performance analysis rather than control design. This can be done by switching from a coefficient-based approach, such as that presented above, to a component modeling method, the latter being based on computational fluid dynamics theory. In detail, each vehicle geometry, with its specific angle of attack and sideslip, is taken into consideration when computing the hydrodynamic forces/moments. This increased computational effort makes it possible to capture some dynamic effects, such as the vortex-induced roll moment, not justifiable with the coefficient-based approach.

Table 43.4 UUVs: possible instrumentation

Sensor	Measured variable
Inertial system	Linear acceleration and angular velocity
Pressure meter	Vehicle depth
Frontal sonar	Distance from obstacles
Vertical sonar	Distance from the bottom
Ground speed sonar	Relative velocity vehicle/bottom
Current meter	Relative velocity vehicle/current
Global positioning system	Absolute position at the surface
Compass	Orientation
Acoustic baseline	Absolute position in known area
Vision systems	Relative position/velocity
Acoustic Doppler current profiler	Water current at several positions

The control plant model is usually a simplified model that captures the most important parts of the dynamics. The most accurate model of the vehicle should be used for prediction and motion simulation.

43.2.2 Sensor Systems

Underwater vehicles are equipped with a sensor system devoted to enabling motion control as well as accomplishing the specific mission it has been commanded to complete. In the latter case, sensors developed for chemical/biological measurements or mapping may be installed, which is beyond the scope of this chapter.

AUVs need to operate underwater most of the time; one of the major problems with underwater robotics is in the localization task due to the absence of a single, proprioceptive sensor to measure the vehicle position. The global position system (GPS) cannot be used underwater. Redundant multisensor systems are commonly combined using state estimation or sensor fusion techniques to provide fault detection and tolerance capability to the vehicle. Table 43.4 lists the types of sensors and the corresponding variable measured commonly available for unmanned underwater vehicles (UUVs).

The sensors that can be found on an underwater vehicle are:

- Compass. A gyrocompass can provide an estimate of geodetic north accurate to a fraction of a degree. Magnetic compasses can provide estimates of magnetic north with an accuracy of less than 1° if carefully calibrated to compensate for magnetic disturbances from the vehicle itself. Tables or models can be used to convert from magnetic north to geodetic north.
- Inertial measurement unit (IMU). An IMU provides information about the vehicle's linear acceleration and angular velocity. These measurements are combined to form estimates of the vehicle's attitude including an estimate of geodetic (true) north from the most complex units. In most cases, for slow-moving underwater vehicles, an independent measurement of the vehicle's velocity is also required to produce accurate estimates of the translational velocity or relative displacement.
- Depth sensor. Measuring the water pressure gives the vehicle's depth. At depths beyond a few hundred meters, the equation of state of seawater must be invoked to produce an accurate depth estimate based on the ambient pressure [43.21]. With a high-quality

Table 43.5 JHUROV instrumentation

Measured variable	Sensor	Precision	Update rate
3-DOF vehicle position	SHARP acoustic transponder	0.5 cm	10 Hz
Depth	Foxboro/ICT model n. 15	2.5 cm	20 Hz
Heading	Litton LN200 IMU Gyro	0.01°	20 Hz
Roll and pitch	KVH ADGC	0.1°	10 Hz
Heading	KVH ADGC	1°	10 Hz

Table 43.6 ODIN III sensors summary

Measured variable	Sensor	Update rate
xy vehicle position	8 sonars	3 Hz
Depth	Pressure sensor	30 Hz
Roll, pitch, and yaw	IMU	30 Hz

sensor, these estimates are reliable and accurate, giving a small error of order 0.01%.

- Altitude and forward-looking sonar. These are used to detect the presence of obstacles and distance from the seafloor.
- Doppler velocity log (DVL). By processing reflected acoustic energy from the seafloor and the water column from three or more beams, estimates of vehicle velocity relative to the seafloor and relative water motion can be obtained. Bottom-tracking velocity estimates can be accurate to ≈ 1 mm/s.
- Global positioning system (GPS). This is used to localize the vehicle while on the surface to initialize or reduce drift of estimates from an IMU/DVL combination. GPS only works at the surface.
- Acoustic positioning. A variety of schemes exist for determining vehicle position using acoustics. Long-baseline navigation can determine the position of the vehicle relative to a set of acoustic beacons anchored to the seafloor or on the surface through range estimates obtained from acoustic travel times. Ultrashort-baseline navigation uses phase information to determine direction from a cluster of hydrophones; this is most often used to determine the direction of the vehicle (in two dimensions) from a surface support vessel, which is then combined with an acoustic travel-time measurement to produce an estimate of relative vehicle position in spherical coordinates. These techniques will be discussed later in the localization section.

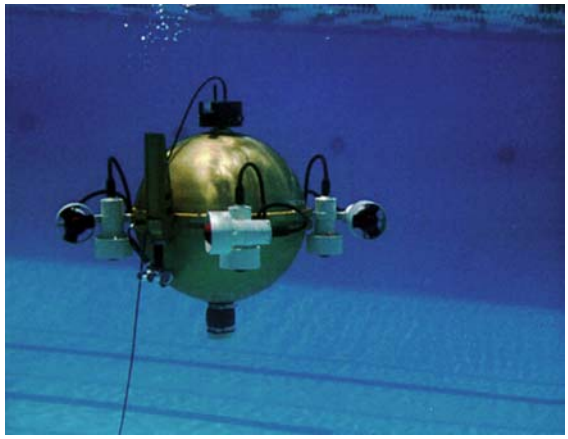

Fig. 43.3 The fully actuated AUV ODIN (courtesy of the Autonomous Systems Laboratory, University of Hawaii, http://www.eng.hawaii.edu/~asl/)

- Vision systems. Cameras can be used to obtain estimates of relative, and in some cases absolute, motion using a type of simultaneous localization and mapping (SLAM) algorithm [43.22] and used to perform tasks such as visual tracking of pipelines, station keeping, visual servoing or image mosaicking.

As an example, Table 43.5 reports some data from the instrumentation of the ROV developed at the John Hopkins University [43.23], and Table 43.6 some data from the AUV ODIN III [43.24]. Reference [43.25] shows some data fusion results with a redundant sensorial system mounted on the AUV Oberon, while reference [43.26] reviews advances in navigation technology.

43.2.3 Actuating Systems

Marine vehicle are generally propelled by means of thrusters or hydrojets. In the case of ROVs with structural pitch–roll stability, there are usually four thrusters that provide holonomic mobility to the four remained DOFs, in particular, the depth is often decoupled and the vehicle is controlled on a plane in the surge, sway, and yaw DOFs. Those vehicles, being underactuated, cannot easily be used for interactive control by means of a manipulator due to the impossibility of counteracting the generalized forces exchanged with the manipulator's base; in such case, six or more thrusters are required. AUVs generally have a torpedo-like shape and are used for mapping/exploration. They are propelled using one or two thrusters parallel to the fore–aft direction and

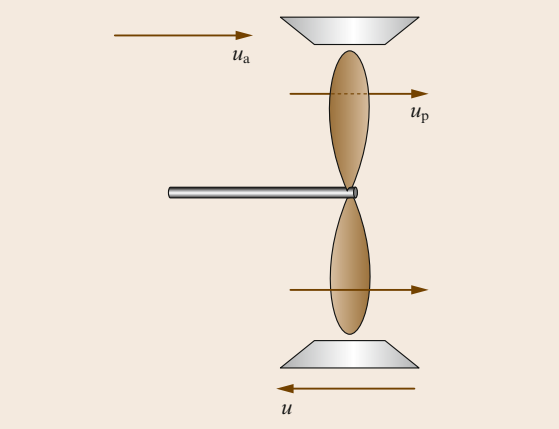

Fig. 43.4 Ambient water and axial flow velocities affecting thruster behavior

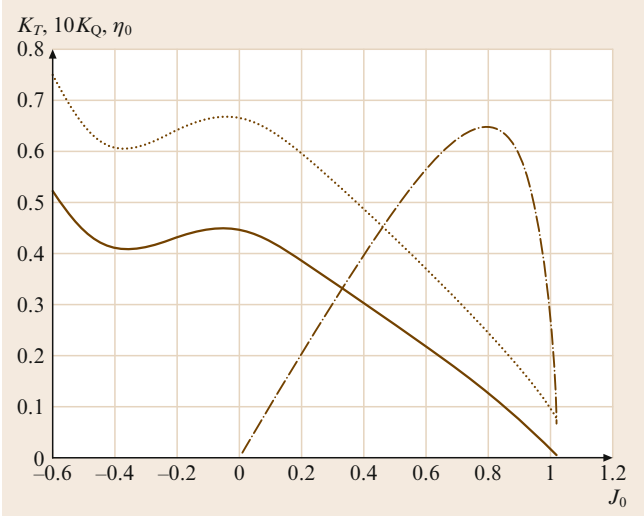

Fig. 43.5 Values of K_T (*solid*), $10K_Q$ (*dotted*), and η_0 (*dash-dotted*) as a function of J_0 [43.27]

a fin and a rudder; this kind of propulsion is obviously nonholonomic and experiences a loss of mobility at low velocities. Hydrojets, also known as pump jets or water jets, are systems that create a jet of water for propulsion; they have certain advantages over thrusters such as a higher power density and usability in shallow water, but can provide thrust in one direction only.

Several efforts have been made to accurately and efficiently describe the mathematical model of a thruster; [43.28] reports a *one-state* model where the state is n, the propeller shaft speed. In [43.29] a *two-state* model is proposed to take into account the experimentally observed overshoot in the thrust; together with n, the additional state variable is u_p, the axial flow velocity in the propeller disc. In [43.30] a thruster model incorporating the effects of rotational fluid velocity and inertia on thruster responses is presented together with a method for experimentally determining nonsinusoidal lift/drag curves. A *three-state* model is described in [43.31]:

$$\begin{aligned} J_m\dot{n} + K_n n &= \tau - Q \,, \\ m_f\dot{u}_p + d_{f0}u_p + d_f\left|u_p\right|(u_p - u_a) &= T \,, \\ (m - X_{\dot{u}})\dot{u} - X_u u - X_{u|u|}u\,|u| &= (1-t)T \,, \end{aligned}$$

where J_m is the moment of inertia for the dc-motor/propeller, K_n is the linear motor damping coefficient, τ is the motor control input, Q is the propeller torque, m_f is the mass of water in the propeller control volume, u_p is the axial flow velocity in the propeller disc, d_{f0} and d_f are the linear and quadratic damping coefficients for control volume, respectively, u_a is the ambient water velocity, T is the propeller thrust, and t is the thrust deduction number (Fig. 43.4). In the case of steady-state motion, i. e., $\dot{u} = 0$, the ambient water velocity u_a is related to the surge by the *wake fraction number* w as:

$$u_a = (1-w)u \,. \tag{43.28}$$

Notice also that the unmeasured variable u_p can be estimated using a nonlinear observer [43.31].

The *outputs* of the nonlinear three-state dynamic systems are the thrust T and the torque Q, which are functions of several variables; in the following, unsteady flow effects such as air suction, cavitation, the in-and-out-of-water (Wagner), boundary layer, and gust (Kuessner) effects will be neglected. This leads to a quasi-steady representation of the model:

$$T = \rho D^4 K_T(J_0) n\,|n| \,, \tag{43.29}$$

$$Q = \rho D^5 K_Q(J_0) n\,|n| \,, \tag{43.30}$$

where D is the propeller diameter and $K_T(J_0)$ and $K_Q(J_0)$ are the thrust and torque coefficients, respectively. The latter are function of the advance ratio J_0

$$J_0 = \frac{u_a}{nD} \,. \tag{43.31}$$

The open-water propeller efficiency in undisturbed water is given as the ratio of the work done by the propeller in producing a thrust force divided by the work required to overcome the shaft torque:

$$\eta_0 = \frac{u_a\,T}{2\pi n Q} = \frac{J_0}{2\pi}\cdot\frac{K_T}{K_Q} \,. \tag{43.32}$$

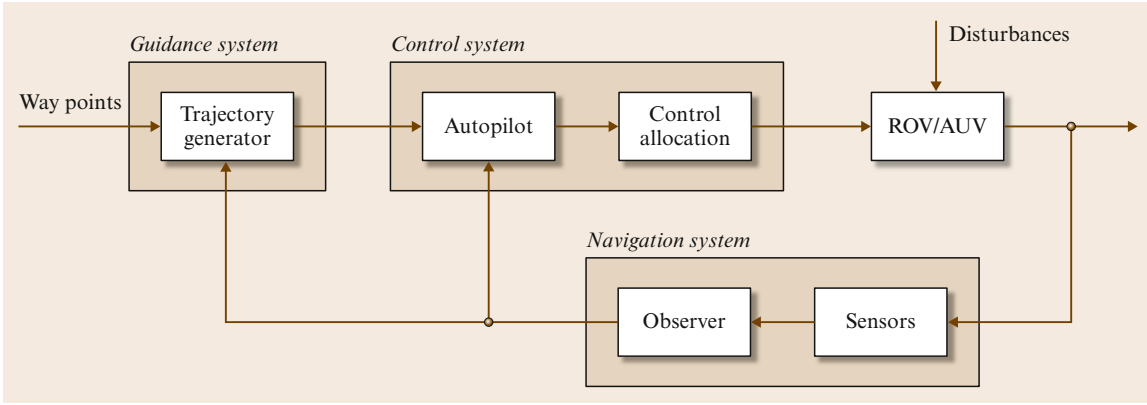

Fig. 43.6 Guidance, navigation, and control for an autonomous marine vehicle

Figure 43.5 shows the values of K_T, K_Q, and η_0 as functions of the advance ratio for the Wageningen B4-70 propeller [43.27].

Controlling a marine vehicle usually requires that desired forces/moments act on the vehicle's body; these generalized forces are mapped into desired thrusts to be provided by the propellers. There is, thus, a nontrivial control problem in that the motors are required to provide the appropriate propeller shaft speed n that satisfies the nonlinear relationship with the thrust T presented above.

To enable robustness with respect to possible failures, the actuating system is often redundant. In this case, the problem of allocation of the desired force/moment acting on the vehicle among the thrusters must also be solved. Reference [43.32] reports a survey of control allocation methods of ships and underwater vehicles.

43.2.4 Mission Control System

The mission control system (MCS) can be considered as the highest-level process running during an AUV's mission; it is responsible for achieving several control objectives. At the highest level it works as an interface between the operator, accepting his instructions in a higher-level language and decomposing those instructions into mission tasks according to the implemented software architecture. The mission tasks are generally concurrent and their handling depends on the vehicle state and environmental conditions; it is therefore the MCS that handles the tasks, eventually suppressing, sequencing, modifying, and prioritizing them. An MCS is also usually equipped with a graphical user interface (GUI) to report the mission state to the operator.

As for most advanced robotics applications, an efficient MCS should allow the use of complex robotic systems by users that do not necessarily know all of their technical details. An overview relevant to underwater mission control is given in [43.33], which includes an interesting classification of the MSCs in use in several laboratories according to which four major AUV control architectures were identified: the hierarchical, heterarchical, subsumption, and hybrid.

From a mathematical point of view, the MCS generally needs to be designed in order to be able to address hybrid dynamical systems, i. e., handling both event-driven and time-driven processes. In [43.34], e.g., the MSC developed at the Portuguese Instituto Superior Técnico (IST), named CORAL, is implemented by resorting to a Petri-net-based architecture that properly handles all the necessary tasks in order to manage navigation, guidance and control, sensing, communications, etc.

The motion-oriented operating system (MOOS), designed at the Massachusetts Institute of Technology, is a software tool capable of executing and coordinating a multitude of subsea operations. The MSC developed at the Naval Postgraduate School is in the framework of the behavioral control organized in three layers [43.35]; it is based on PROLOG, an artificial intelligence language for predicate logic.

43.2.5 Guidance and Control

The terms guidance and control can be defined as [43.7]:

Guidance is the action of determining the course, attitude, and speed of the vehicle, relative to

some reference frame (usually the Earth), to be followed by the vehicle,

Control — is the development and application to a vehicle of appropriate forces and moments for operating point control, tracking, and stabilization. This involves designing the feedforward and feedback control laws.

Figure 43.6 shows the corresponding block diagram, in which the navigation component is also outlined.

Guidance of Underwater Vehicles

Guidance algorithms may benefit from a wide range of inputs, overall mission information, real-time operator input, environmental measured data such as the ocean current, environmental topological information such as a bathymetric map, exteroceptive sensors for obstacle avoidance, and obviously the vehicle state as output from the navigation system.

The vehicle may be required to follow a path, i. e., a curve geometrically represented in two or three dimensions, or a trajectory, i. e., a path with a specific time law assigned. Moreover, when the desired position is constant, the problem is called set-point regulation or maneuvering. The guidance problem is commonly decomposed into simple subtasks of lower dimension: an attitude control problem and a path control. Moreover, attitude is usually considered as a simple depth set-point with null roll and pitch and the path is usually a line in the horizontal plane.

One of the most common guidance approaches is based on the generations of way-points. Those are usually stored in a database and are used to generate the vehicle path/trajectory; a *passing* velocity, in fact, may be defined together with the Cartesian coordinates of the points. The simplest way to connect the way-points is to use the segments connecting two successive way-points. Efficient way-point-based guidance approaches need to take into account the presence of the current and the eventual nonholonomicity of the vehicle [43.36]. A technique for adaptively tracking bathymetric contours by proper generation of way-points is presented in [43.37]; environment information is acquired by mean of a single vertical sonar. An alternative method is based on *line-of-sight* guidance [43.38–40]. In this case, the heading control is computed by considering as input the angle formed by the vector from the vehicle to the next way-point rather than requiring the vehicle to exactly follow the line segment between the current and the following way-point. Special care needs to be paid to the docking maneuver with algorithms designed on the scope [43.41].

By combining vision-based guidance with a neurocontroller trained by reinforcement learning, in [43.42], an algorithm aimed at a hold station on a reef or swimming along a pipe has been presented. In [43.43] guidance for AUVs specifically involved in a predeployment survey of the sea bottom and visual inspection of pipelines is given. Reference [43.44] reports a specific guidance system aimed at mine avoidance for AUVs. Based on a three-dimensional discretization of the environment, the path-planning technique consists of computing a safe path avoiding the unsafe cells of the map. Due to the poor manoeuvrability at low speed under some conditions, the vehicle has to make a 360° turn to avoid stopping and to map the environment close to it before generating a safe path.

A deep discussion on guidance for surface and underwater vehicles can be found in [43.3, 7].

Control of Underwater Vehicles

Control of underwater vehicles needs to consider the different operating conditions and actuating configurations in which a submerged vehicle is required to operate. In particular, there are three main control problems.

- An AUV traveling at high speed (> 1 m/s) generally equipped with at least one thruster aligned in the fore–aft direction and at least two control surfaces (stern and rudder).
- An underactuated ROV, with high metacentric stability, i. e., structurally stable in roll and pitch, and equipped with at least four thrusters.
- A fully actuated AUV equipped with at least six trusters.

AUVs equipped with control surfaces are underactuated vehicles mainly used for survey/exploration missions. Inheriting the common practice of submarine control, they are not allowed to perform arbitrary motions in six DOFs but are rather designed to perform specific movements such as: cruising along a given direction at constant depth, steering at constant depth, or diving. Marine experience and mathematical insight, in fact, demonstrate that these movements are lightly coupled in dynamic terms. For these vehicles, moreover, specific manoeuvres such as homing or docking require special capabilities [43.41]. This requires the design of vehicles that are structurally stable in the roll DOF. Cruising requires control of the surge velocity $u(t)$; steering requires control of the sway velocity $v(t)$ and the yaw DOF $r(t)$, $\psi(t)$, diving requires control of the

heave DOF $\omega(t)$, $z(t)$ and the pitch DOF $q(t)$, $\theta(t)$. The simplest configuration of actuators that can control an AUV through these movements is composed of one thruster aligned along the fore–aft direction, one stern, and one rudder; the control variables, thus, are the propeller speed and the deflection of the fins. Several approaches can then be considered to solve this control problem, among them, in [43.45] the sliding mode control is proposed, while [43.46] presents an adaptive sliding mode control for the diving manoeuvre. Reference [43.17] reports a successful implementation of multivariable sliding mode control on the NPS AUV II, later also implemented on the NPS ARIES AUV [43.47]. As the model of an AUV traveling at high speed is nonlinear and coupled, the tuning of the parameters is mainly based on a linearized model around the working conditions.

From a descriptive point of view, an ROV is mainly a box-shaped underwater vehicle equipped with tools such as a video camera or robot manipulator, while its payload is often variable depending on the task. It is remotely operated and physically connected to another vehicle, either an underwater or a surface vessel. It is mainly designed to travel at low speed and it is structurally stable in roll and pitch, while its depth, surge, sway, and yaw are independently controllable. Due to the absence of a specific shape, the varying payload, and the relatively low required performances, it is common to control a ROV by means of single-input single-output (SISO) controllers. Moreover, the PID approach is often used due to its simplicity. A two-layer guidance and control architecture for the ROV Romeo is given in [43.48].

Control of a fully actuated AUV in six DOFs is needed in the case of, e.g., an interaction task performed by a manipulator mounted on a vehicle; the latter, in fact, needs to provide all the force/moment components in order to counteract the presence of the manipulator dynamically. This problem is kinematically similar to the problem of controlling a satellite in six DOFs; the underwater environment, however, makes it significatively different from the dynamic point of view. In kinematic terms the main issue is in implementing a suitable policy for orientation control; any three-parameter representation of orientation, in fact, experiences representation singularities (Chap. 1). This problem may be overcome by resorting to a redundant representation of the orientation such as the quaternion. Most of the six-DOF controllers proposed in the literature are based on (43.16), which model the simplified effect of the hydrodynamic terms and which have very similar properties as the equations of motion of an industrial manipulator. Based on this, it is obviously possible to find a collection of approaches inherited from classical robotics, see, e.g., [43.3, 7] for some examples. In [43.49], some specific considerations for the underwater environment lead to a quaternion-based, adaptive controller; it is worth noticing that adaptive control requires a suitable, and simplified, expression for the hydrodynamic terms. In [43.50] a comparison among several 6-DOF controllers is made.

43.2.6 Localization

Localization in the underwater environment can be a complex task, mainly due to the absence of a single external sensor that gives the vehicle position such as, e.g., the GPS for outdoor ground vehicles; moreover, the environment is often poorly structured.

One of the most reliable methods is based on the use of acoustic systems such as the baseline systems: the long-baseline system (LBL), the short-baseline system (SBL), and the ultrashort-baseline system (USBL). These systems are based on the presence of a transceiver mounted on the vehicle and a variable number of transponders located in known positions. The transceiver's distance from each transponder can be measured via the measurement of an echo delay; from this information the position of the vehicle can be calculated by basic triangulation operations. The USBL can be used with a single transponder, which is usually mounted on a surface ship whose position is measured by GPS.

Another localization system is called terrain-aided navigation and is based on the use of terrain elevation maps; bathymetric maps are available, especially in the case of well-known locations such as harbors where they usually have a resolution of ≈ 1 m. In this case, the vehicle position is obtained by filtering the information coming from a downward-looking sonar. In [43.51], a particle filter approach was used to localize an AUV in Sydney harbor.

Moving vehicles may be equipped with an IMU or DVL in order to measure its velocity and/or acceleration. This data can then be integrated to estimate the vehicle position. This kind of information is subject to the drift phenomenon and may not be reliable for long-duration runs or may become cost ineffective if accurate IMU devices are needed.

Relative localization can be obtained by resorting to any device that provides information about the relative position of the vehicle with respect to the environment,

even in the absence of a map. In this case, by filtering the distance measurements taken along the motion, the vehicle's position can be measured. This is the case, e.g., of sonar or vision-based localization techniques [43.52].

Often, the techniques presented above are used together in a redundant system and the effective position is obtained by resorting to sensor fusion techniques such as the Kalman filtering approach.

Simultaneous Localization and Mapping

Simultaneous localization and mapping (SLAM), also known as concurrent mapping and localization (CML), is a wide topic in mobile robotics. The problem can be formulated as the requirement for a mobile robot to be placed in an unknown environment and progressively build a map while locating itself inside the map. Chapter 37 discusses this topic in detail. For the marine environment an additional issue arises due by the large-scale map that needs to be used for long-duration missions; [43.53] implements a decoupled stochastic mapping to handle this computational problem in an extended Kalman filter. Terrain-aided navigation with the use of a scanning sonar is implemented in [43.54]. Reference [43.55] uses long-baseline range measurements as the input for a nonlinear least-squares approach solved by the Gauss–Newton method; both the initially unknown position of the transponders and the vehicle position are estimated. An interesting survey on navigation and SLAM for underwater vehicles is given in [43.26].

43.2.7 Underwater Manipulation

A manipulator may be mounted on an AUV or a ROV in order to accomplish interaction operations. In this case, the vehicle needs to be fully actuated to counteract the forces and moments generated by the manipulator's base. By considering a manipulator with n links, thus six DOFs, the underwater vehicle manipulator system (UVMS) is a $(6+n)$-DOF robotic system whose velocity vector is

$$\boldsymbol{\zeta} = (\boldsymbol{v}_1^\top \ \boldsymbol{v}_2^\top \ \dot{\boldsymbol{q}}^\top)^\top , \tag{43.33}$$

where $\boldsymbol{q} \in \mathbb{R}^n$ is the vector collecting the manipulator joints positions.

Repeating the same considerations as for an underwater vehicle, it is possible to write the equations of motions of an UVMS in matrix form as

$$\boldsymbol{M}(\boldsymbol{q})\dot{\boldsymbol{\zeta}} + \boldsymbol{C}(\boldsymbol{q}, \boldsymbol{\zeta})\boldsymbol{\zeta} + \boldsymbol{D}(\boldsymbol{q}, \boldsymbol{\zeta})\boldsymbol{\zeta} + \boldsymbol{g}(\boldsymbol{q}, \boldsymbol{R}_{\mathrm{B}}^{\mathrm{I}}) = \boldsymbol{\tau} , \tag{43.34}$$

where $\boldsymbol{M} \in \mathbb{R}^{(6+n)\times(6+n)}$ is the inertia matrix, including added mass terms, $\boldsymbol{C}(\boldsymbol{q}, \boldsymbol{\zeta})\boldsymbol{\zeta} \in \mathbb{R}^{6+n}$ is the vector of the Coriolis and centripetal terms, $\boldsymbol{D}(\boldsymbol{q}, \boldsymbol{\zeta})\boldsymbol{\zeta} \in \mathbb{R}^{6+n}$ is the vector of dissipative effects, and $\boldsymbol{g}(\boldsymbol{q}, \boldsymbol{R}_{\mathrm{I}}^{\mathrm{B}}) \in \mathbb{R}^{6+n}$ is the vector of gravity and buoyancy effects. The relationship between the generalized forces $\boldsymbol{\tau}$ and the control input is given by:

$$\boldsymbol{\tau} = \begin{pmatrix} \boldsymbol{\tau}_{\mathrm{v}} \\ \boldsymbol{\tau}_q \end{pmatrix} = \begin{pmatrix} \boldsymbol{B}_{\mathrm{v}} & \boldsymbol{0}_{6\times n} \\ \boldsymbol{0}_{n\times 6} & \boldsymbol{I}_n \end{pmatrix} \boldsymbol{u} = \boldsymbol{B}\boldsymbol{u} , \tag{43.35}$$

where $\boldsymbol{u} \in \mathbb{R}^{p_{\mathrm{v}}+n}$ is the vector of the control input. Notice that, while for the vehicle a generic number $p_{\mathrm{v}} \geq 6$ of control inputs is assumed, for the manipulator it is supposed that n joint motors are available.

Under this hypothesis, which can be considered as reasonable at low velocity, it holds that:

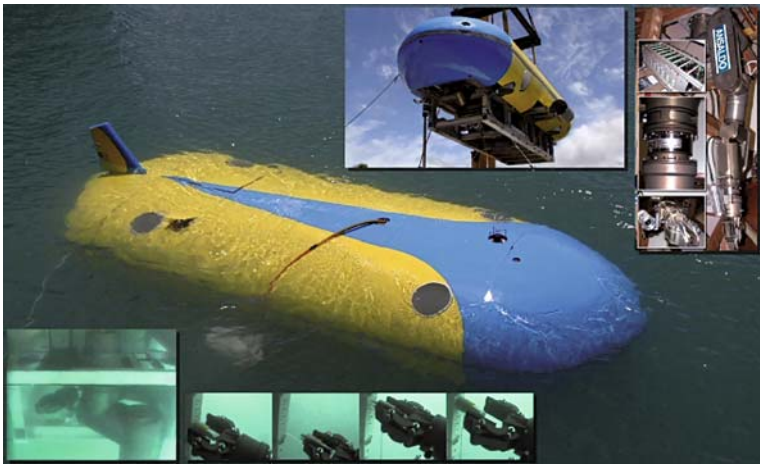

Fig. 43.7 An underwater vehicle–manipulator system: SAUVIM (courtesy of Autonomous Systems Laboratory, University of Hawaii, http://www.eng.hawaii.edu/~asl/)

- the inertia matrix $\boldsymbol{M}$ of the system is symmetric and positive definite;
- for a suitable choice of the parametrization of $\boldsymbol{C}$ and if all the single bodies of the system are symmetric, $\dot{\boldsymbol{M}} - 2\boldsymbol{C}$ is skew symmetric;
- the matrix $\boldsymbol{D}$ is positive definite.

In [43.19] the mathematical model written with respect to the Earth-fixed-frame vehicle position and the manipulator end-effector can be found. However, it must be noted that, in this case, a six-dimensional manipulator is considered in order to have a square Jacobian to work with; moreover, kinematic singularities need to be avoided.

The equations of motion of UVMSs in matrix form presented in (43.34) are formally similar to the equations of motion of ground fixed manipulators (Chap. 2) for which a wide control literature exists. This has suggested a suitable translation/implementation of existing control algorithms. However, some differences, crucial from the control aspect, need to be underlined. UVMSs are complex systems characterized by several strong constraints:

- uncertainty in the model knowledge, mainly due to the poor knowledge about the hydrodynamic effects
- the complexity of the mathematical model
- the kinematic redundancy of the system
- the difficulty in controlling the vehicle in hovering, mainly due to poor thruster performance
- the dynamic coupling between the vehicle and the manipulator
- the low bandwidth of the sensor readings

In 1996 *McLain* et al. [43.56] presented a control law for UVMSs with some interesting experimental results conducted at the Monterey Bay Aquarium Research Institute (MBARI). A one-link manipulator was mounted on the OTTER vehicle controlled in all six DOFs by means of eight thrusters. A coordinated control system was then implemented to improve the tracking errors of the end effector.

The monograph [43.50] is focused on the modeling and control issues of such systems, and can be considered as a reference for further reading. Moreover, interaction with the environment is also discussed.

Currently, remotely operated manipulator are standard equipment for several underwater ROVs. However, autonomous manipulation is still a research challenge. Figure 43.7 shows the SAUVIM vehicle, one of the first semiautonomous underwater vehicle manipulator systems, developed at the Autonomous Systems Laboratory, University of Hawaii. A similar research project, ALIVE, was funded by the Fifth Framework Program of the European Community [43.2].

43.2.8 Fault Detection/Tolerance

Generally, AUVs must operate over long periods of time in unstructured environments in which an undetected failure could cause the loss of the vehicle. Failure detection and a fault-tolerant strategy are required to determine whether a mission must be terminated in the safest manner possible or if the vehicle can continue in a diminished capacity. An example is the case of the arctic mission of Theseus [43.57].

In the case of the use of ROVs, a skilled human operator is in charge of commanding the vehicle; a failure detection strategy is then of help in the human decision-making process. Based on the information detected, the operator can decide on vehicle rescue or to terminate the mission by, e.g., turning off a thruster.

Fault detection is the process of monitoring a system in order to recognize the presence of a failure; fault isolation or diagnosis is the capability to determine which specific subsystem is subject to failure. Often in the literature there is a certain overlap in the use of these terms. Fault tolerance is the capability to complete the mission in the case of the failure of one or more subsystems; it is also known as fault control, fault accommodation, or control reconfiguration. In the following the terms fault detection/tolerance will be used.

The characteristics of a fault detection scheme are the capability to isolate the detected failure, sensitivity in terms of the magnitude of the failure that can be detected, and robustness in the sense of the capability to continue working properly in non-nominal conditions. The requirements of a fault-tolerant scheme are reliability, maintainability, and survival. The common concept is that, to overcome the loss of capability due to a failure, a kind of redundancy is required in the system.

In this section, a survey of existing fault-detection and fault-tolerant schemes for underwater vehicles is presented. For these specific systems, if proper strategies are applied, a hardware/software (HW/SW) sensor or thruster failure can be successfully handled. In some conditions, the fault-detection scheme must also be able to diagnose some external abnormal working conditions such as a multipath phenomena affecting the echo-sounder system. It is worth noticing that, for autonomous systems such as AUVs, space systems or aircraft, a fault-tolerant strategy is necessary to safely recover the damaged vehicle and, obviously, there is no

panic button in the sense that the choice of turning off the power or activating some kind of brake is not available.

Most fault-detection schemes are model based [43.58, 59] and consider the dynamic relationship between the actuators and vehicle behavior or the specific input–output thruster dynamics. In general, fault-detection/tolerance theory has been applied to the specific case of the underwater environment even if only a few papers report experimental results; see [43.60] for a survey on this topic.

Most fault-tolerant schemes consider a thruster-redundant vehicle that, after a fault has occurred in one of its thrusters, is still actuated in six DOFs. Based on this assumption a reallocation of the desired forces on the vehicle over the working thrusters is performed [43.61]. Of interest is also the study of reconfiguration strategies if the vehicle becomes underactuated.

Possible Failures

Underwater vehicles are currently equipped with several sensors in order to provide information about their localization and velocity. The problem is not easy. No single, reliable sensor is available that gives the required position/velocity measurement, or information about the environment such as the presence of obstacles. For this reason the use of sensor fusion by, e.g., a Kalman filtering approach, is a common technique to provide the controller with the required variables. This structural redundancy can be used to provide fault-detection capabilities to the system.

For each of the sensors listed in Sect. 43.2.2 failure can consist of an output of zero if, e.g., there is an electrical trouble, or a loss of meaning. It can be considered as sensor failure also an external disturbance such as a multipath reading of the sonar that can be interpreted as a sensor fault and correspondingly detected.

Thruster blocking occurs when a solid body is present between the propeller blades. It can be checked by monitoring the current required by the thruster. This was observed, e.g., during the Antarctic mission of Romeo [43.62], in that case caused by a block of ice. During the same mission a thruster also flooded with water. The consequence was an electrical dispersion, causing an increasing blade rotation velocity and thus a thruster force higher then desired.

A possible consequence of different failures of the thrusters is the zeroing of the blade rotation. The thruster in question thus simply stops working. This has been intentionally experienced during experiments with, e.g., ODIN [43.59, 61], Roby 2 [43.58], and Romeo [43.62].

Other failures include a hardware/software crash or the occurrence of fin sticking or loss. A very common type of failure involves the loss of electrical isolation due to seawater intrusion into underwater electrical cables or connectors. Such a condition can be detected through a technique called ground-fault monitoring. Should this occur, electrical power must be removed from the affected device.

43.2.9 Multiple Underwater Vehicles

A growing research effort has recently been devoted to developing strategies to design coordinated control for underwater vehicles. The use of multiple AUVs, in fact, might improve overall mission performance as well as provide greater tolerance to failures (Chap. 40). Specific applications of this method in the underwater environment might include the naval mine countermeasure problem, harbor monitoring, and inspection, exploration, and mapping of large areas. AUVs might be coordinated with one or more surface vessels or connected to ground or aerial vehicles to form a coordinated network of heterogeneous autonomous robots.

Beside several institutions that have developed simulation packages for multiple-AUV operations, the use of real multiple AUVs is being considered for the adaptive sampling and forecasting plan of the Autonomous Ocean Sampling Network, formed by several research institutions such as (for the robotic components) Caltech, MBARI, Princeton, and WHOI [43.63]. Adaptive sampling is also being investigated at the Autonomous Systems and Controls Laboratory of Virginia Tech, which has developed five AUVs [43.64]. The Australian National University is currently working on a shoal of small, autonomous robots, named Serafina [43.65]. At Instituto Superior Técnico (IST), work is ongoing on the coordination between an AUV and a catamaran [43.66], i. e., a multirobot system constituted by heterogeneous autonomous vehicles.

43.3 Applications

Underwater robots currently play prominent roles in a number of scientific, commercial, and military tasks. Remotely teleoperated vehicles are very well established in all these areas, and are becoming increasingly auto-

mated to relieve the burden on human operators and to improve performance. Increasingly, autonomous underwater vehicles are finding application in these areas as well. Presently, AUVs are used almost exclusively for survey work, but sampling and other intervention tasks are becoming more feasible. Additionally, the line between ROVs and AUVs continues to blur, as systems that have the best properties of both evolve.

The offshore oil and gas industry relies heavily on ROVs for installation, inspection, and servicing of platforms, pipelines, and subsea production facilities. As the search for oil and gas goes deeper, this trend can only continue. The Marine Technology Society estimates that there are over 435 *work-class* ROVs operating in the commercial offshore industry today. AUVs are now beginning to appear in the commercial offshore industry for survey tasks, and concepts for hybrid systems that can perform intervention tasks are now appearing. The goal is not only for these robotic vehicles to replace human divers or human-occupied vehicles, but to enable an entire new generation of subsea equipment that is serviced without intervention by drill ships or other heavy-lifting vessels. This holds the prospect of greatly reduced cost.

Scientific demand for ROVs and AUVs is also increasing dramatically. Scientific applications for ROVs include survey, inspection, and sampling tasks previously performed by human-occupied submersibles or towed vehicles. While ROVs operating for science are not nearly as numerous as those in the offshore oil and gas industry, they are becoming commonplace. Most nations involved in global seafloor studies have several vehicles. Like the vehicles for the commercial offshore sector, these vehicles are becoming increasingly automated. High-quality electronic imaging, including high-definition television, is becoming increasingly common. Scientific ROVs are now equipped with sophisticated sampling devices for sampling animals, microbes, caustic hydrothermal vent fluids, and a variety of rock samples. Moreover, ROVs are also used to deploy and operate seafloor experiments, which can involve difficult tasks such as drilling and delicate placement of instruments.

ROVs have also emerged as powerful tools for investigating underwater shipwrecks and other cultural sites. Applications include forensic investigations of modern shipwrecks to determine the cause of sinking, archaeology, and salvage. For archaeology, the goals are the same as for excavation on land: detailed mapping followed by careful excavation. Beyond diver depths, ROVs are the preferred method for these investigations. Great progress has been made in the detailed mapping phase, and capabilities for excavation are evolving. Unfortunately, the same technology also opens the possibility for shipwrecks to be looted for financial gain, which usually results in the loss of the most valuable historical information.

After a long period of skepticism, AUVs are now accepted for scientific tasks. Presently, AUVs most often perform mapping tasks while tended by a vessel. Specific mapping tasks include seafloor bathymetry, sidescan sonar imaging, magnetic field mapping, hydrothermal vent localization, and photo surveys. AUVs have been shown to improve productivity and data quality compared to towed and tethered systems. They have also operated in environments where no other means of gathering data is possible, such as under ice shelves. Likewise, the increasing availability of sophisticated in situ chemical sensors, biological sensors, and mass spectrometers now allows AUVs to build spatial and temporal maps of environmental features that could previously only be studied by bringing samples back to the laboratory. Plans are now underway for AUVs that can dock to subsea moorings or observatory nodes to recharge batteries and receive new instructions.

The military has always been a leader in the development of underwater robotic capabilities. They pioneered ROVs for tasks such as recovering test weapons and deep-sea salvage, and present-day commercial and scientific ROVs have descended directly from these early systems. Likewise, military interests are presently pushing AUV technology very hard. Many different countries operate AUVs for military surveys, gathering environmental data as well as searching for hazards such as mines. An operational success was achieved in surveying for mines in the Persian Gulf harbor of Umm Qasr using REMUS vehicles. AUVs in development will not only be able to detect mines, but to disable them. Bolder, more innovative concepts are also in development. These include networks of AUVs that can act as extensions of conventional surface vessels and submarines, enabling surveillance over wide areas for extended periods of time at costs far less than could be achieved with conventional surface vessels, submarines, and aircraft. These developments will rely on improvements in acoustic communications, energy systems, sensors, and onboard intelligence that will likely find their way into commercial and scientific practice.

43.4 Conclusions and Further Reading

The underwater environment is extremely hostile for human engineering activities. In addition to high pressures and hydrodynamic forces that are both nonlinear and unpredictable, water is not an appropriate media for electromagnetic communication except at short ranges. This pushes underwater technology to rely on acoustic communication and positioning systems that are characterized by low bandwidth. On the other hand, the ocean is extremely important for numerous human activities from the commercial, cultural, and environmental points of view.

Research on underwater robotic applications is active both from the technological and methodological aspects. The power endurance of commercially AUVs is currently up to 50 h; this will increase as energy-storage devices improve. Improved energy and power capability will enable longer missions, higher speeds, or better/additional sensors such as, e.g., more powerful lighting for underwater video/photography. The current trend for the price of AUVs prices is downward, with more and smaller research institutions building or buying AUVs to enrich their research results; moreover the setup of multiple-AUV systems is becoming cost effective. The goal is to develop fully autonomous, reliable, robust, decision-making AUVs.

There are a number of technology issues that are needed in order to improve AUV capabilities: to increase the underwater bandwidth of current acoustic modems, to increase onboard power to handle larger tools and interact more strongly with the environment, to create AUVs with significant hovering capability to allow better interaction, and to enable easier launch and recovery.

In the near future, the ROV/AUV dichotomy will likely become less prominent, with a variety of systems appearing that have attributes of both systems:

- For offshore oil and gas intervention tasks, a vehicle could transit to the work site as a self-powered, fully autonomous vehicle, then dock to the work site. Utilizing energy and communications infrastructure at the work site, the vehicle could then be operated much like a conventional ROV.
- Battery-operated ROVs can communicate with the surface by very lightweight fiber-optic links, enabling the mobility of an AUV but with a high-bandwidth connection to skilled human operators for complex intervention or scientific sampling tasks.
- Acoustic and optical data links can provide moderate to high communication bandwidths over short ranges, enabling human supervision without any tether restrictions. At longer ranges, more modest acoustic bandwidths are available.

These developments make marine robotics a challenging engineering problem with strong connections to several engineering domains. Sending an autonomous vehicle into an unknown and unstructured environment with limited online communication requires some onboard intelligence and the ability for the vehicle to react in a reliable way to unexpected situations [43.67, 68].

A major challenge concerning underwater robotics is the interaction with the environment by means of one or more manipulators. Autonomous UVMSs are still the object of research; the current trend is in developing the first semiautonomous robotic devices, which might be acoustically operated; moreover, if physically possible, the capability to dock to the structure where the intervention is needed might significatively simplify the control. The final aim might be to develop a completely autonomous UVMS, able to localize the intervention site, recognize the task to be performed, and act on it without docking to the station and without human intervention. This might make it possible to perform missions that are currently impossible such as autonomous archaeological intervention at deep sites. This would also enable the oil and gas industry to significatively decrease costs and risks to humans.

For further reading on the topic of underwater systems, the reader is referred to several survey articles, including [43.5, 26, 32, 33, 60]. Additionally, several journals cover oceanic engineering topics, including robotics aspects. A variety of symposia and workshops have been held on a regular basis. Some books/monographs treating marine robotics are [43.3, 7, 8, 16, 50].

References

43.1 J. Yuh, S.K. Choi, C. Ikehara, G.H. Kim, G. McMurty, M. Ghasemi-Nejhad, N. Sarkar N., K. Sugihara: Design of a semi-autonomous underwater vehicle for intervention missions (SAUVIM), (1998) pp. 63–68

43.2 P. Marty: ALIVE: An autonomous light intervention vehicle, Advances in Technology for Underwater Vehicles Conference, Oceanology Int. (2004)

43.3 T.I. Fossen: *Marine Control Systems, Guidance, Navigation and Control of Ships, Rigs and Underwater Vehicles* (Marine Cybernetics AS, Trondheim 2002)

43.4 S. Bennett: A brief history of automatic control, IEEE Contr. Syst. Mag. **16**(3), 17–25 (1996)

43.5 J. Yuh, M. West: Underwater robotics, J. Adv. Robot. **15**(5), 609–639 (2001)

43.6 SNAME: Marine engineers: nomenclature for treating the motion of a submerged body through a fluid, Techn. Res. Bull. **1–5**, (1950)

43.7 T.I. Fossen: *Guidance and Control of Ocean Vehicles* (Wiley, New York 1994)

43.8 O.M. Faltinsen: *Sea Loads on Ships and Offshore Structures* (Cambridge Univ Press, Cambridge 1990)

43.9 J. Yuh: Modeling and control of underwater robotic vehicles, IEEE Trans. Syst. Man Cybern. **20**, 1475–1483 (1990)

43.10 T.I. Fossen, A. Ross: Guidance and control of unmanned marine vehicles, IEEE Contr. Eng. Series (Peregrinus, Stevengce 2006) pp. 23–42

43.11 W.E. Cummins: The impulse response function and ship motions, Techn. Rep. **1661**, *David Taylor Model Basin, Hydromechanics Laboratory* (DTIC, Washington 1962)

43.12 T.F. Ogilvie: Recent progress towards the understanding and prediction of ship motions, 5th Symposium Naval Hydrodynamics (1964) pp. 3–79

43.13 T. Perez, T.I. Fossen: Time-domain models of marine surface vessels for simulation and control design based on seakeeping computations, 7th IFAC Conf. Manoeuvring Contr. Marine Craft (IFAC, Lisbon, 2006)

43.14 T.I. Fossen: A nonlinear unified state-space model for ship maneuvering and control in a seaway, J. Bifurc. Chaos **15**(9), 2717–2746 (2005)

43.15 M. Nahon: Determination of undersea vehicle hydrodynamic derivatives usingthe USAF Datcom, Proc. Oceans Conf. (Victoria 1993) pp. 283–288

43.16 J.N. Newman: *Marine Hydrodynamics* (MIT Press, Cambridge 1977)

43.17 A.J. Healey, D. Lienard: Multivariable sliding mode control for autonomous diving and steering of unmanned underwater vehicles, IEEE J. Oceanic Eng. **18**, 327–339 (1993)

43.18 B. Stevens, F. Lewis: *Aircraft Control and Simulations* (Wiley, New York 1992)

43.19 I. Schjølberg, T.I. Fossen: Modelling and control of underwater vehicle-manipulator systems, 3rd IFAC Conf. Manoeuvring Contr. Marine Craft (IFAC, Southampton 1994) pp. 45–57

43.20 E.A. de Barros, A. Pascoal, E. de Sea: Progress towards a method for predicting AUV derivatives, 7th IFAC Conf. Manoeuvring Contr. Marine Craft (IFAC, Lisbon 2006)

43.21 N.P. Fofonoff, R.C. Millard: *Algorithms for Computation of Fundamental Properties of Seawater*, 44th edn. (UNESCO Technical papers in marine science, Paris 1983)

43.22 R. Eustice, H. Singh, J.J. Leonard, M. Walter, R. Ballard: Visually navigating the RMS Titanic with SLAM information filters, Proc. Robot. Sci. Syst. (Cambridge 2005) pp. 57–64

43.23 D.A. Smallwood, L.L. Whitcomb: Adaptive identification of dynamically positioned underwater robotic vehicles, IEEE Trans. Contr. Syst. Technol. **11**(4), 505–515 (2003)

43.24 S. Zhao, J. Yuh: Experimental study on advanced underwater robot control, IEEE Trans. Robot. **21**(4), 695–703 (2005)

43.25 S. Majumder, S. Scheding, H.F. Durrant-Whyte: Multisensor data fusion for underwater navigation, Robot. Autonom. Syst. **35**(2), 97–108 (2001)

43.26 J.C. Kinsey, R.M. Eustice, L.L. Whitcomb: A survey of underwater vehicle navigation: recent advances and new challenges, 7th IFAC Conf. Manoeuvring Contr. Marine Craft (IFAC, Lisbon 2006)

43.27 W.P.A. Van Lammeren, J. van Manen, M.W.C. Oosterveld: The Wageningen B-screw series, Trans. SNAME **77**, 269–317 (1969)

43.28 D.R. Yoerger, J.G. Cooke, J.J. Slotine: The Influence of thruster dynamics on underwater vehicle behavior and their incorporation into control system design, IEEE J. Oceanic Eng. **15**, 167–178 (1990)

43.29 A.J. Healey, S.M. Rock, S. Cody, D. Miles, J.P. Brown: Toward an improved understanding of thruster dynamics for underwater vehicles, IEEE J. Oceanic Eng. **20**(4), 354–361 (1995)

43.30 L. Bachmayer, L.L. Whitcomb, M.A. Grosenbaugh: An accurate four-quadrant nonlinear dynamical model for marine trhusters: theory and experimental validation, IEEE J. Oceanic Eng. **25**, 146–159 (2000)

43.31 T.I. Fossen, M. Blanke: Nonlinear output feedback control of underwater vehicle propellersusing feedback form estimated axial flow velocity, IEEE J. Oceanic Eng. **25**(2), 241–255 (2000)

43.32 T.I. Fossen, T.I. Johansen: A survey of control allocation methods for ships and underwater vehicles, 14th IEEE Mediterriaen Conf. Contr. Autom. (Ancona 2006) pp. 1–6

43.33 K.P. Valavanis, D. Gracanin, M. Matijasevic, R. Kolluru: Control architecture for autonomous underwater vehicles, IEEE Contr. Syst. **17**, 48–64 (1997)

43.34 P. Oliveira, A. Pascoal, V. Silva, C. Silvestre: Mission control of the MARIUS AUV: system design, implementation, and sea trials, Int. J. Syst. Sci. **29**(10), 1065–1080 (1998)

43.35 D. Brutzman, M. Burns, M. Campbell, D. Davis, T. Healey, M. Holden, B. Leonhardt, D. Marco, D. McClarin, B. McGhee: NPS Phoenix AUV software integration and in-water testing, Autonomous

Underwater Vehicle Technol. AUV'96 (1996) pp. 99–108
43.36 A.P. Aguiar, A.M. Pascoal: Dynamic positioning and way-point tracking of underactuated AUVs in the presence of ocean currents, 41st IEEE Conf. Decision Contr. (Las Vegas 2002) pp. 2105–2110
43.37 A.A. Bennett, J.J. Leonard: A behavior-based approach to adaptive feature detection and following with autonomous underwater vehicles, IEEE J. Oceanic Eng. **25**(2), 213–226 (2000)
43.38 M. Breivik, T.I. Fossen: Principles of guidance-based path following in 2D and 3D, 44th IEEE Conf. Decision Contr. 8th Eur. Contr. Conf. (Sevilla 2005)
43.39 F.A. Papoulias: Bifurcation analysis of line of sight vehicle guidance using sliding modes, Int. J. Bifurc. Chaos **1**(4), 849–865 (1991)
43.40 R. Rysdyk: UAV path following for constant line-of-sight, Proc. 2nd AIAA Unmanned Unlimited Syst. Technol. Operations – Aerospace (San Diego 2003)
43.41 M.D. Feezor, F.Y. Sorrel, P.R. Blankinship, J.G. Bellingham: Autonomous underwater vehicle homing/docking via electromagnetic guidance, IEEE J. Oceanic Eng. **26**(4), 515–521 (2001)
43.42 D. Wettergreen, A. Zelinsky, C. Gaskett: Autonomous guidance and control for an underwater robotic vehicle, Int. Conf. Field Service Robot. (Pittsburgh 1999)
43.43 G. Antonelli, S. Chiaverini, R. Finotello, R. Schiavon: Real-time path planning and obstacle avoidance for RAIS: an autonomous underwater vehicle, IEEE J. Oceanic Eng. **26**(2), 216–227 (2001)
43.44 J.C. Hyland, F.J. Taylor: Mine avoidance techniques for underwater vehicles, IEEE J. Oceanic Eng. **18**, 340–350 (1993)
43.45 D.R. Yoerger, J.J. Slotine: Robust trajectory control of underwater vehicles, IEEE J. Oceanic Eng. **10**, 462–470 (1985)
43.46 R. Cristi, F.A. Pappulias, A. Healey: Adaptive sliding mode control of autonomous underwater vehicles in the dive plane, IEEE J. Oceanic Eng. **15**(3), 152–160 (1990)
43.47 D.B. Marco, A.J. Healey: Command, control and navigation experimental results with the NPS ARIES AUV, IEEE J. Oceanic Eng. **26**(4), 466–476 (2001)
43.48 M. Caccia, G. Veruggio: Guidance and control of a reconfigurable unmanned underwater vehicle, Cont. Eng. Prac. **8**(1), 21–37 (2000)
43.49 G. Antonelli, F. Caccavale, S. Chiaverini, G. Fusco: A novel adaptive control law for underwater vehicles, IEEE Trans. Contr. Syst. Technol. **11**(2), 221–232 (2003)
43.50 G. Antonelli: Underwater robots, Motion and force control of vehicle-manipulator systems. In: *Tracts in Advanced Robotics*, 2nd edn., ed. by G. Antonelli (Springer, Berlin, Heidelberg 2006)
43.51 S.B. Williams: A terrain aided tracking algorithm for marine systems, 4th Int. Conf. Field Service Robot. (2003) pp. 55–60
43.52 M. Dunbabin, P. Corke, G. Buskey: Low-cost vision-based AUV guidance system for reef navigation, IEEE Int. Conf. Robot. Autom. (New Orleans 2004) pp. 7–12
43.53 J.J. Leonard, H.J.S. Feder: Decoupled stochastic mapping, IEEE J. Oceanic Eng. **26**(4), 561–571 (2001)
43.54 S. Williams, G. Dissanayake, H. Durrant-Whyte: Towards terrain-aided navigation for underwater robotics, Adv. Robot. **15**(5), 533–549 (2001)
43.55 P. Newman, J. Leonard: Pure range-only sub-sea SLAM, IEEE Int. Conf. Robot. Autom. (Taipei 2003) pp. 1921–1926
43.56 T.W. McLain, S.M. Rock, M.J. Lee: Experiments in the coordinated control of an underwater arm/vehicle system, Auton. Robot. **3**(2), 213–232 (1996)
43.57 J.S. Ferguson, A. Pope, B. Butler, R. Verrall: Theseus AUV – two record breaking missions, Sea Technol. Mag. **40**, 65–70 (1999)
43.58 A. Alessandri, M. Caccia, G. Veruggio: Fault detection of actuator faults in unmanned underwater vehicles, Cont. Eng. Prac. **7**, 357–368 (1999)
43.59 K.C. Yang, J. Yuh, S.K. Choi: Fault-tolerant system design of an autonomous underwater vehicle – ODIN: an experimental study, Int. J. Syst. Sci. **30**(9), 1011–1019 (1999)
43.60 G. Antonelli: A survey of fault detection/tolerance strategies for AUVs and ROVs. Recent advances. In: *Fault Diagnosis and Tolerance for Mechatronic Systems*, Springer Tracts in Advanced Robotics, ed. by F. Caccavale, L. Villani (Springer, Berling, Heidelberg 2002) pp. 109–127
43.61 T.K. Podder, G. Antonelli, N. Sarkar: An experimental investigation into the fault-tolerant control of an autonomous underwater vehicle, J. Adv. Robot. **15**, 501–520 (2001)
43.62 M. Caccia, R. Bono, G. Bruzzone, G. Bruzzone, E. Spirandelli, G. Veruggio: Experiences on actuator fault detection, diagnosis and accomodation for ROVs, Int. Symp. Unmanned Untethered Submersible Technol. (Durham, New Hampshire 2001)
43.63 E. Fiorelli, P. Bhatta, N.E. Leonard, I. Shulman: Adaptive sampling using feedback control of an autonomous underwater glider fleet, Int. Symp. Unmanned Untethered Submersible Technol. (Durham, New Hampshire 2003)
43.64 C.J. Cannell, D.J. Stilwell: A comparison of two approaches for adaptive sampling of environmental processes using autonomous underwater vehicles, Proc. Oceans Conf. (Brest 2005) pp. 1514–1521
43.65 S. Kalantar, U. Zimmer: Distributed shape control of homogeneous swarms of autonomous underwater vehicles, Auton. Robot. **22**(1), 37–53 (2006)

43.66 A. Pascoal, C. Silvestre, P. Oliveira: Vehicle and mission control of single and multiple autonomous marine robots. In: *Advances in Unmanned Marine Vehicles*, IEEE Control Engineering, ed. by G. Roberts, R. Sutton (Peregrinus, New York 2006) pp. 353–386

43.67 J. Yuh: Exploring the mysterious underwater world with robots, 6th IFAC Conf. Manoeuvring Contr. Marine Craft (IFAC, Girona 2003)

43.68 T. Ura: Steps to intelligent AUVs, 6th IFAC Conf. Manoeuvring Contr. Marine Craft (IFAC, Girona 2003)